Available online at www.sciencedirect.com

ScienceDirect

Geochimica et Cosmochimica Acta 312 (2021) 180–193

Geochimica et Cosmochimica Acta

www.elsevier.com/locate/gca

Zn uptake by illite and argillaceous rocks

Rainer Dähn *, Bart Baeyens, Maria Marques Fernandes

Paul Scherrer Institut, Villigen PSI, CH-5232, Switzerland

Received 1 December 2020; accepted in revised form 1 July 2021; Available online 6 July 2021

Abstract

The uptake of Zn by Illite du Puy (IdP) and two argillaceous rocks, Opalinus Clay (OPA) and Boda Claystone (BODA) was investigated. The uptake of Zn by illite was studied in 0.1 M NaCl at near-neutral pH and Zn loadings varying from 2.1 to 42 mmol/kg. The Zn uptake by the two argillaceous rock systems was carried out in 0.1 M NaCl at pH 7.2 and in their respective porewaters at pH 8.0 to evaluate the influence of porewater composition. The Zn loadings varied from 1.8 to 86 mmol/kg and 1.7 to 60 mmol/kg for OPA and BODA, respectively.

The simplified "bottom-up approach" to predict the uptake of Zn to natural rocks with different clay mineral contents and porewater compositions was tested. This approach was found to be applicable in the argillaceous rock systems at low Zn equilibrium ($[Zn]_{eql}$) concentrations below 10^{-7} M. However, at $[Zn]_{eql}$ above 10^{-7} M, the model calculations clearly underpredicted the sorption data.

The extended X-ray absorption fine structure (EXAFS) results support findings based on wet chemistry calculations using the 2 site protolysis non-electrostatic surface complexation and cation exchange (2SPNE SC/CE) sorption model. In the IdP system with prolonged reaction times of up to two years, formation of Zn precipitates was not observed. This indicates that the Zn surface complexes are stable over a time period of two years, and dissolution and recrystallization processes might not play a significant role in the Zn-IdP uptake process. In addition, the EXAFS results on illite corroborate previous findings on the existence of weak and strong sites types in dioctahedral clay minerals, as assumed in the 2SPNE SC/CE model. In the OPA and BODA systems, precipitation processes could start to begin at metal loadings of 16 mmol/kg and 24 mmol/kg, respectively. The differences between argillaceous rock samples prepared in NaCl and porewater are modest indicating that in the case of Zn the clay minerals play a predominant role in the uptake process, and that the effects originating from the porewater are minor. Furthermore, despite the differences in mineralogy, both argillaceous rocks show the same uptake behaviour, indicating that the clay minerals are predominantly responsible for the sorption at low and the precipitation processes at higher Zn concentrations. The study demonstrates how results on "pure" systems such as IdP can be transferred to predict the uptake by argillaceous rocks at low sorbate concentrations.

Keywords: Zn; Argillaceous rocks; Illite; Opalinus Clay; Boda Claystone; Uptake

1. INTRODUCTION

Zn is a metal of high density, belonging to the group of post-transition elements and is an essential micronutrient for plants, animals and humans. The abundance of Zn in the lithosphere is 75 mg/kg and in non-polluted soils in the range of 10–300 mg/kg (Pais and Jones Jr, 1997). In animal metabolism, it is of importance as a constituent of many enzymes and hence deficiencies appear as results of insufficient enzyme activities. In plant growth, Zn is crucial for enzymes such as dehydrogenases and peptidases (Mengel and Kirkby, 1978). Plants, however, have a much higher sensitivity to Zn toxicity compared to animals, which

* Corresponding author.
E-mail address: rainer.daehn@psi.ch (R. Dähn).

https://doi.org/10.1016/j.gca.2021.07.001
0016-7037/

in turn serves as an automatic protection against Zn accumulation in the food chain (De Haan and Zwerman, 1976).

Leeper (1972) and Chaney (1973) recommend that the maximum toxic Zn metal content in soils should not exceed Zn equivalent fractions equal to 5 % of the cation exchange capacity (CEC) of soils at pH $\leq$ 6.5. The availability of Zn in soils depends on several factors of which pH is one of the main controlling factor (Chumbley, 1971; Chaney, 1973). Phyllosilicates, especially clay minerals, play a dominant role in many soils and sediments (Sposito, 2008). They exhibit singular crystal structures (size, composition and arrangement) which confer their exceptional bulk physical and chemical properties. Due to these unique properties, clay minerals control to a large extent most important characteristics of many soils and sediments (*e.g.* cation exchange, texture, swelling, pH buffering and retention of micronutrients or (radio-)contaminants). The 2:1-clay minerals such as illite, smectite, illite/smectite mixed layers and vermiculite are often major components of soils, sediments and argillaceous rocks. The understanding of the uptake of transition and heavy metals on clay minerals and argillaceous rocks is important to maintain a sustainable environment and remediate contaminated sites.

In the case of the deep geological disposal of radioactive waste, the adsorption of radionuclides on clay-rich sediments is one of the main retardation mechanisms on which the safety assessment relies. Therefore, in many waste management programmes, argillaceous rocks are foreseen as potential host formations for the deep geological disposal of radioactive waste (Bonin, 1998; Andra, 2001; Ondraf/Niras, 2001; Nagra, 2002; Lázár and Máthé, 2012). Their high content in clay minerals (up to 50 wt.%) is an important characteristic from the viewpoint of host rock selection.

Development of sorption models on pure reference minerals is crucial for the prediction of the fate of metal ions in complex geochemical environments (Davis et al., 1998). One modelling approach (so-called component additive or bottom-up) assumes that the retention of cationic elements in complex mineral/groundwater systems can be quantitatively described by considering sorption on the individual mineralogical components, and by using the corresponding models developed on each mineral to predict their behaviour (Payne et al., 2013). In a simplified bottom-up approach with application to clay mineral-rich environments, it is assumed that only the 2:1-clay mineral content controls the overall metal uptake and that illite/smectite mixed layers behave similar to illite (Bradbury and Baeyens, 2011; Marques Fernandes et al., 2015).

Few studies addressed the sorption of divalent metals on argillaceous rocks (e.g. Bradbury and Baeyens, 2011; Chen et al., 2014; Marques Fernandes et al., 2015). Marques Fernandes et al. (2015) used the bottom-up approach mentioned above with the **2** **s**ite **p**rotolysis **n**on-**e**lectrostatic surface **c**omplexation and **c**ation **e**xchange (2SPNE SC/CE) model for illite (Bradbury and Baeyens, 2009a) to blind predict the sorption isotherms of Ni and Co, amongst other elements in complex porewater on the same Opalinus Clay (OPA) and Boda Claystone (BODA) samples as used in the present study. In their modelling, they considered the total clay mineral content (illite, illite/smectite mixed layers). One outcome was that the predictions for the divalent metals Co and Ni on both argillaceous samples follow the same trend. At Co/Ni equilibrium concentrations below 10^{-6}–10^{-7} M, the experimental data and the blind predictive model agree rather well, even so Ni on OPA was slightly underpredicted. At Ni equilibrium concentrations above 10^{-6} M (however below any solubility limits such as Co/Ni-hydroxides, -oxides or -carbonates) the model clearly underpredicted the sorption for both elements on both rock samples. Ni extended X-ray absorption fine structure (EXAFS) data suggested that the formation of surface precipitates could explain the mismatch between modelling and experimental data (Marques Fernandes et al., 2015). The modelling approach does not consider the formation of precipitates implying that in environments where the uptake of metals is governed by such processes the adsorption model is no longer applicable. The surface precipitate formed could not be unambiguously identified because of the rather noisy quality of the spectra. Chen et al. (2014) investigated the retention of Ni on the argillaceous Callovo-Oxfordian (COx) formation. Their model gives a satisfactory estimation of Ni adsorption on COx. At higher Ni loadings they could observe by EXAFS the neoformation of Ni phyllosilicates. They concluded that retention processes induced by non-clay phases such as calcite should not be neglected for samples with low clay mineral content.

Illite is a major component of argillaceous rocks such as OPA and BODA (Bradbury and Baeyens, 2011; Breitner et al., 2015). Recently, Montoya et al. (2018) studied the sorption of Zn amongst other divalent metals on illite du Puy (IdP) and implemented the 2SPNE SC/CE sorption model for illite (Bradbury and Baeyens, 2009a, b) with the selectivity coefficients and surface complexation constants for Zn on illite.

Molecular scale studies on the uptake of Zn on clays, soil minerals and sediments are sparse. Manceau et al. (2002) has studied, amongst other heavy metals, the speciation of Zn on soils and sediments by synchrotron X-ray techniques. Using polarized extended X-Ray Absorption Fine Structure (P-EXAFS) spectroscopy, Schlegel et al. (2001c) and Dähn et al. (2011) showed the formation of Zn surface complexes located at edge sites of trioctahedral hectorite and dioctahedral montmorillonite, respectively. More generally, EXAFS has demonstrated that divalent metals such as Co and Ni forms inner-sphere complexes at edge sites of the 2:1 dioctahedral clay mineral montmorillonite at near-neutral pH and low metal loadings (Schlegel et al., 1999; Dähn et al., 2003). With increasing Ni or Zn loading, several studies observed the neoformation of Ni/Zn-phyllosilicates (Dähn et al., 2001; Schlegel et al., 2001a; Dähn et al., 2002b; Schlegel and Manceau, 2006).

In the present study, a similar approach as used in Dähn et al. (2011) was applied by combining wet chemistry experiments with modelling to produce representative sorption samples for EXAFS spectroscopy to investigate the structural environment of Zn on illite, OPA and BODA as a function of Zn surface loading. Additionally, Zn isotherms were measured in batch sorption experiments on OPA and

BODA in their respective synthetic porewaters. The illite model developed by Montoya et al. (2018) was used to blind predict the experimental data. EXAFS measurements were performed to structurally characterize the surface species formed and consequently, to identify the different retention mechanisms controlling the uptake of Zn on illite as well as on OPA and BODA with increasing Zn loadings. The overall aim of this study is to test the applicability of an adsorption model in complex natural rock systems together with EXAFS measurements.

2. SORPTION MODELLING

The sorption of Zn on illite in 0.1 M NaCl and on both argillaceous rocks in 0.1 M NaCl and synthetic porewaters (SPW) was quantitatively described with the 2SPNE SC/CE model using the non-adjustable site capacities and protolysis constants for the amphotheric edge sites of Na-illite (Bradbury and Baeyens, 2009a; Table SI-1) and the parameters summarized in Table 1 as derived by Montoya et al. (2018). For the application to the argillaceous rocks, the site capacities in the illite model were scaled to the 2:1-clay mineral content of the given rock. The sorption of Zn was calculated in the respective porewaters compositions i.e., considering the aqueous speciation with the thermodynamic data given in Table 1. A more detailed description of the applied bottom-up approach is given in Marques Fernandes et al. (2015).

3. MATERIALS AND METHODS

3.1. Illite, Boda Claystone and Opalinus Clay

3.1.1. Illite

The source material used in the present study was Illite du Puy (IdP) (Gabis, 1958) collected from an 80 m thick Oligocene geological formation in the region of Le Puy-en-Velay (Haute-Loire), France. IdP samples were crushed, then powdered in a mortar and sieved until the clay passed the size of 240 mesh (≤63 μm) using Retsch equipment. The applied clay mineral purification procedures have been described in detail elsewhere (Poinssot et al., 1999; Bradbury and Baeyens, 2009a). The cation exchange capacity (CEC) of the purified IdP was measured by isotope dilution technique (Baeyens and Bradbury, 2004). CEC measurements on different IdP clay batches at neutral pH in $5{\cdot}10^{-3}$ M $CsNO_3$ at solid to liquids ratios (S:L) of ~12 g/L yielded an average Cs-CEC value of 225 ± 10 meq/kg (Marques Fernandes and Baeyens, 2019). The quantitative elemental composition of IdP determined by ICP-MS (Inductively Coupled Plasma Mass Spectrometry) analysis after borate fusion indicates an intrinsic structural Zn content of 2.9 mmol per kg illite.

3.1.2. Opalinus Clay and Boda Claystone

The same argillaceous rock samples as in the study of Marques Fernandes et al. (2015) were used. The OPA sample originates from a geothermal well in Schlattingen in northeastern Switzerland and was cored at a depth of 938 m below surface (SLA-938).

The BODA sample was obtained from the Gorica block (borehole Ib-4 at a depth of 540 m) located in West-Mecsek Mountains, South Western Hungary. Two distribution areas of upper Permian sedimentary sequence of BODA are known in West-Mecsek Mountains, the peri-anticlinal structure of the West-Mecsek Anticline Block and the Gorica Block. A detailed description of the geology of the BODA formation can be found in Lázár and Máthé (2012).

The mineralogical composition of OPA and BODA samples used in this study is given in Table 2. The elemental analysis of both argillaceous rocks indicates an intrinsic Zn content of 4.1 mmol/kg in OPA and 2.2 mmol/kg in BODA.

3.2. Sorption experiments

3.2.1. Zn sorption on IdP

A Zn sorption isotherm was carried out on Na-IdP at pH 7.2 in 0.1 M $NaClO_4$ over a large range of Zn concentrations (10^{-8} M ≤ $[Zn]_{eql}$ ≤ 10^{-2} M). A series of Zn solutions covering the concentration range required were prepared at pH 7.2 in 0.1 M $NaClO_4$ background electrolyte. The clay suspension and Zn solutions were set to pH 7.2 using MOPS buffer. The solutions were labelled with ^{65}Zn radiotracer. The maximum Zn concentrations used in the sorption isotherm measurements at pH 7.2 was 10^{-5} M, two orders of magnitude below the predicted solubility limits for $ZnO/Zn(OH)_2$ (Baes and Mesmer, 1976). Aliquots of conditioned Na-IdP suspensions were pipetted into 40 ml centrifuge tubes followed by additions of the labelled $ZnCl_2$

Table 1
Surface complexation and cation exchange reactions of Zn on strong sites, weak sites and planar sites of illite and the corresponding surface complexation constants and selectivity coefficient (Montoya et al., 2018).

Surface complexation reactions on strong sites (2 mmol/kg)	log ^{S}K
$\equiv S^{S}OH + Zn^{2+} \rightarrow \equiv S^{S}OZn^{+} + H^{+}$	2.1
$\equiv S^{S}OH + Zn^{2+} + H_2O \rightarrow \equiv S^{S}OZnOH^{0} + 2H^{+}$	−6.4
$\equiv S^{S}OH + Zn^{2+} + 2H_2O \rightarrow \equiv S^{S}OZn(OH)_2^{-} + 3H^{+}$	−15.0
Surface complexation reactions on weak sites (40 mmol/kg)	**log ^{W}K**
$\equiv S^{W1}OH + Zn^{2+} \rightarrow \equiv S^{W1}OZn^{+} + H^{+}$	−1.4
$\equiv S^{W1}OH + Zn^{2+} + H_2O \rightarrow \equiv S^{W1}OZnOH^{0} + 2H^{+}$	−7.7
Cation exchange on the planar sites (225 meq kg^{-1})	**log K_c**
$2Na^{+}\text{-IdP} + Zn^{2+} \rightarrow Zn^{2+}\text{-IdP} + 2Na^{+}$	0.6

Table 2
Mineralogical composition of Opalinus Clay SLA-938 and Boda Claystone Ib-4-540 (Breitner et al., 2015) samples and CEC values (Marques Fernandes et al., 2015).

Mineral	OPA (SLA-938)	BODA (Ib-4-540)
Illite	17 wt. %	–
Illite/smectite mixed layer	30 wt.%	–
Illite/muscovite	–	50 wt.%
Chlorite	6 wt.%	–
Kaolinite	21 wt.%	–
Quartz	9 wt.%	8 wt.%
Calcite	7 wt.%	8 wt.%
Dolomite/ankerite	2 wt.%	–
K-feldspar/albite	1 wt.%	17 wt.%
Siderite	6 wt.%	–
Pyrite	0.9 wt.%	–
Hematite	–	6 wt.%
Analcime	–	10 wt.%
CEC	0.183 eq·kg^{-1}	0.113 eq·kg^{-1}

solutions. The samples were shaken end-over-end for 7 days inside a glove box. Subsequently, they were removed from the glove box and centrifuged at high speed using a Beckman Coulter Avanti™ J30i High-Performance Centrifuge (1 h at 108,000*g* max.) before returning them to the glove box for pH measurement. Aliquots of the supernatant were taken for radio assay of ^{65}Zn using a Canberra Packard Cobra Quantum counter together with standard labelled solutions. The results of these measurements were published by Montoya et al. (2018).

3.2.2. Zn sorption on Opalinus Clay and Boda Claystone

For the sorption experiments on OPA and BODA, the rock samples were ground and sieved in order to obtain crushed rock material <63 μm.

Prior to the sorption measurements, the crushed argillaceous rock samples were conditioned with the respective synthetic OPA and BODA porewaters (Table 3). The procedure was the same for both rocks and is described in detail in Marques Fernandes et al. (2015). The concentrations of the major elements Na, K, Mg, Ca, Sr, Si and S (SO_4) in the liquid phases of the conditioned OPA and BODA batches remained essentially constant during the conditioning procedures and are very similar to the synthetic porewaters.

Table 3
Composition of the synthetic porewaters (SPW) for BODA and OPA used in the Zn sorption measurements (Marques Fernandes et al., 2015).

Parameter	OPA SPW	BODA SPW
pH	7.8 ± 0.2	8.0 ± 0.2
Ionic strength (M)	$2.3{\cdot}10^{-1}$	$3.3{\cdot}10^{-2}$
Elements	Concentration (M)	
Na (total)	$1.6{\cdot}10^{-1}$	$1.7{\cdot}10^{-2}$
K (total)	$3.2{\cdot}10^{-3}$	$1.8{\cdot}10^{-4}$
Mg (total)	$8.7{\cdot}10^{-3}$	$2.4{\cdot}10^{-3}$
Ca (total)	$1.2{\cdot}10^{-2}$	$3.1{\cdot}10^{-3}$
Cl (total)	$1.6{\cdot}10^{-1}$	$2.3{\cdot}10^{-2}$
CO_3^{2-}/HCO_3^-	$5.4{\cdot}10^{-4}$	$6.1{\cdot}10^{-4}$
SO_4^{2-}	$2.4{\cdot}10^{-2}$	$1.9{\cdot}10^{-3}$
Si	$7.1{\cdot}10^{-5}$	$1.8{\cdot}10^{-4}$

3.2.2.1. Zn sorption isotherms. Zn concentration dependent sorption experiments were carried out under aerobic atmospheric conditions. Standard solutions covering Zn initial concentrations between 10^{-8} – 10^{-2} M were prepared in the conditioned synthetic porewaters and were labelled with ^{65}Zn (Eckert & Ziegler Isotope Products, Valencia, California, US). The ^{65}Zn tracer concentration was $6.6{\cdot}10^{-11}$ M in each tracer solution. Aliquots of conditioned rock suspensions were pipetted into 40 ml centrifuge tubes followed by addition of the labelled $ZnCl_2$ solutions. The sorbent concentrations in the experiments were 3.82 g/L and 3.92 g/L for OPA and BODA, respectively. The samples were end-over-end shaken for 1 week followed by centrifugation (1 h at 108′000 g max) for phase separation. 5 ml aliquots of the supernatants were radio assayed in a gamma counter (Canberra Packard Cobra Quantum) and pH was measured.

3.2.2.2. Data presentation. The results of the isotherm sorption experiments are presented as the logarithm of the amount Zn sorbed (log $[Zn]_{ads}$) *vs.* the logarithm of Zn equilibrium concentration in solution (log $[Zn]_{eql}$); $[Zn]_{init}$ is the initial Zn concentration:

$$[Zn]_{ads} = \left([Zn]_{init} - [Zn]_{eql}\right) \cdot \frac{V}{m}$$

3.3. EXAFS sample preparation

For the EXAFS measurements, Zn loaded illite, OPA and BODA samples were prepared in batch sorption experiments in 200 ml polypropylene vessels in a similar way as described in Section 3.2, but in the absence of ^{65}Zn tracer, i.e. only with stable Zn. After equilibration, phase separation of the suspensions was carried out by centrifugation, the supernatants were separated from the wet pastes which were filled into polyethylene sample holders and sealed with Kapton tape. The pH of the supernatants was measured

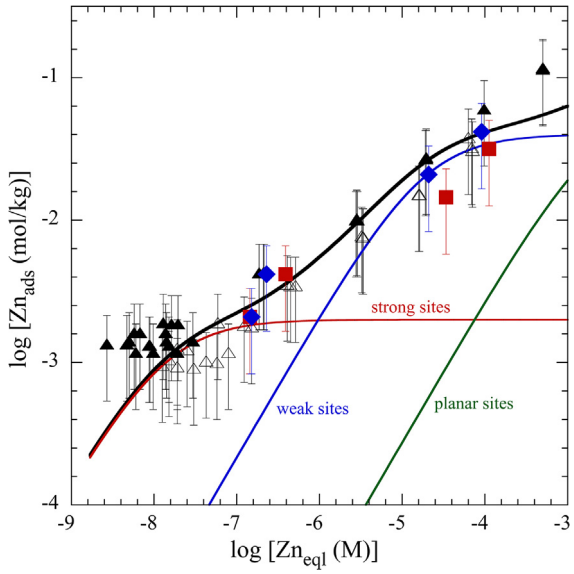

Fig. 1. Zn sorption isotherm in 0.1 M $NaClO_4$ at pH 7.2 on Na-IdP; experimental data from Montoya et al. (2018) (▲); four Zn EXAFS samples (this study) after (■) 1 week of reaction time and (◆) 2 years of reaction time. Model from Montoya et al. (2018): (black line) overall sorption using the 2SPNE SC/CE model; (red line) contribution of strong sites; (blue line) contribution of weak sites; (green line) contribution of planar sites.

and the solutions were analysed for major cations by ICP-OES.

3.3.1. IdP samples

Four IdP samples with increasing Zn loadings (IdP-Zn1 to IdP-Zn-4) were prepared in 0.1 M NaCl at pH 7.2 ± 0.1 (along the Zn IdP reference isotherm, see Fig. 1). The loadings were chosen and optimized based on the 2SPNE SC/CE Zn model on illite, to produce quantitatively well-defined samples in terms of the specific surface composition (e.g., predominantly on strong sites, or weak sites) and with metal loadings high enough to be detectable by EXAFS while low enough for strong sites to be accessed. The samples were investigated spectroscopically after 1 week and 2 years equilibration time, respectively. EXAFS measurements were also performed on Na-IdP without addition of external Zn (IdP-Zn_{incor}) to determine the structure of intrinsic Zn in IdP (see Section 3.1.1). A summary of the experimental details of all the IdP EXAFS samples are given in Table 4. The concentrations of Na, K, Mg, Ca, Al and Si in the supernatants are given in Table SI-2

3.3.2. OPA and BODA samples

In total, 19 different Zn loadings (10 BODA and 9 OPA samples) were prepared in their respective SPW (along the isotherm, see Fig. 3) as well as in 0.1 M NaCl at pH 7.2 (Table 5). Since both argillaceous rocks also contain substantial amounts of intrinsic Zn (see Section 3.1.2), EXAFS measurements were also performed on the "as received" crushed rock material. The equilibration time for the Zn-OPA and Zn-BODA samples was 1 week. The experimental conditions used for the preparation of the rock samples are summarized in Table 5. The concentrations of Na, K, Mg, Ca, Al and Si in the supernatants are given in Table SI-2.

3.4. EXAFS data collection and reduction

The Zn K-edge spectra were collected at the Stanford Synchrotron Radiation Lightsource (SSRL, Menlo Park, CA) at beamline 11-2. All spectra were recorded at room temperature using a Si(220) double crystal LN_2-cooled monochromator and a Canberra 100-pixel Ge solid-state monolith detector. To reduce unwanted fluorescence noise (*i.e.* elastic and Compton scattering) by samples, a Cu filter and Soller slits were used. Energy calibration was performed simultaneously by measuring in transmission mode a Zn foil (9659 eV). Higher order harmonics were rejected by detuning the monochromator by 30 %. Several spectra were averaged to improve the signal to noise ratio.

EXAFS data were reduced using the Athena-Artemis-IFEFFIT package (Newville, 2001; Ravel and Newville, 2005). The Fourier transforms (FT) were obtained from the $k^3\chi(k)$ functions between k = 2.4 – 11 $Å^{-1}$, using a Kaiser-Bessel window function (apodization parameter of 1).

FT peaks of interest were selected and fitted in reciprocal space with the Artemis interface of the IFFEFIT software. Amplitude and phase shifts functions were calculated with FEFF 8.40 (Rehr et al., 1991; Ankudinov et al., 1998), using the montmorillonite structure given by Tsipursky and Drits (1984), in which one Al was replaced by Zn (Dähn et al., 2011). The amplitude reduction factor S_0^2 was set to 0.85 (O'Day et al., 1994; Manceau et al., 1998; Schlegel and Manceau, 2006; Dähn et al., 2011).

Throughout the data analysis, which was performed on the inverse Fourier transforms (FT^{-1}) of the first and second shells, the number of degrees of freedom in the least-squares refinements was reduced by fixing the Debye Waller factor (σ_j) and ΔE_0 (the shift between theoretical and experimental threshold energy) to the value obtained for the lowest concentrated sorption samples. EXAFS distances ($R_{Zn\text{-}j}$) and coordination numbers ($CN_{Zn\text{-}j}$) were allowed to float. It was not possible to fit any of the experimental data of IdP using a Zn—Zn pair and/or a combination of Zn—Zn and Zn-Si/Al pairs. This finding suggests that the substantial formation of a Zn nucleation phase (e.g. $ZnOH_2$, Zn phyllosilicates) can be ruled out under the employed reaction conditions in the IdP uptake system. In the case of OPA and BODA samples at higher loadings, Zn—Zn backscattering pairs were taken into account.

4. RESULTS: ZN-ILLITE

4.1. Zn isotherm on illite

The Zn sorption isotherm (Montoya et al., 2018) in 0.1 M $NaClO_4$ together with the four EXAFS samples (coloured symbols) in 0.1 M NaCl at pH ~ 7 and the modelling are shown in Fig. 1. The EXAFS data follow fairly well the non-linear adsorption isotherm. After two years of equilibration time, a slight increase in sorption is observed at higher $[Zn]_{eql}$ concentrations, however with

Table 4
Experimental details of the IdP EXAFS samples: S:L ratio = 2 g/L in 0.1 M NaCl.

Sample	$[Zn]_{init}$ (M)	$[Zn]_{eql}$ (M)		Zn_{ads} (mmol/kg)		pH
		1 week	2 years	1 week	2 years	
IdP-Zn1	$4.4{\cdot}10^{-6}$	$1.5{\cdot}10^{-7}$	$1.5{\cdot}10^{-7}$	2.1	2.1	7.2
IdP-Zn2	$8.8{\cdot}10^{-6}$	$3.9{\cdot}10^{-7}$	$2.3{\cdot}10^{-7}$	4.2	4.3	7.2
IdP-Zn3	$6.4{\cdot}10^{-5}$	$3.4{\cdot}10^{-5}$	$2.1{\cdot}10^{-5}$	15	21	7.2
IdP-Zn4	$1.8{\cdot}10^{-4}$	$1.1{\cdot}10^{-4}$	$9.1{\cdot}10^{-5}$	32	42	7.2

Table 5
Experimental conditions for OPA and BODA EXAFS samples.

Sample	$[Zn]_{init}$ (M)	$[Zn]_{eql}$ (M)	Zn_{ads} (mmol/kg)	Electrolyte	S:L ratio (g/L)	pH
OPA-NaCl-Zn1	$4.4{\cdot}10^{-6}$	$4.9{\cdot}10^{-7}$	1.8	0.1 M NaCl	2.2	7.2
OPA-NaCl-Zn2	$1.1{\cdot}10^{-5}$	$1.5{\cdot}10^{-7}$	4.9	0.1 M NaCl	2.2	7.2
OPA-NaCl-Zn3	$1.3{\cdot}10^{-4}$	$1.2{\cdot}10^{-6}$	32	0.1 M NaCl	4	7.2
OPA-NaCl-Zn4	$3.5{\cdot}10^{-4}$	$6.2{\cdot}10^{-6}$	86	0.1 M NaCl	4	7.2
OPA-SPW-Zn1	$1.0{\cdot}10^{-5}$	$1.5{\cdot}10^{-7}$	2.1	SPW	4.8	8.0
OPA-SPW-Zn2	$2.7{\cdot}10^{-5}$	$5.2{\cdot}10^{-7}$	5.5	SPW	4.8	8.0
OPA-SPW-Zn3	$8.0{\cdot}10^{-5}$	$2.7{\cdot}10^{-6}$	16	SPW	4.8	8.0
OPA-SPW-Zn4	$1.8{\cdot}10^{-4}$	$7.9{\cdot}10^{-6}$	36	SPW	4.8	8.0
BODA-NaCl Zn1	$4.9{\cdot}10^{-6}$	$1.1{\cdot}10^{-6}$	1.7	0.1 M NaCl	2.2	7.2
BODA-NaCl Zn2	$1.6{\cdot}10^{-5}$	$3.0{\cdot}10^{-7}$	7.1	0.1 M NaCl	2.2	7.2
BODA-NaCl Zn3	$6.4{\cdot}10^{-5}$	$1.1{\cdot}10^{-5}$	24	0.1 M NaCl	2.2	7.2
BODA-NaCl Zn4	$1.8{\cdot}10^{-4}$	$4.8{\cdot}10^{-5}$	60	0.1 M NaCl	2.2	7.2
BODA-SPW-Zn1	$2.1{\cdot}10^{-5}$	$1.5{\cdot}10^{-7}$	4.2	SPW	5	8.0
BODA-SPW-Zn2	$1.2{\cdot}10^{-5}$	$3.6{\cdot}10^{-7}$	5.8	SPW	2	8.0
BODA-SPW-Zn3	$4.9{\cdot}10^{-5}$	$1.9{\cdot}10^{-7}$	9.8	SPW	5	8.0
BODA-SPW-Zn4	$1.2{\cdot}10^{-4}$	$3.2{\cdot}10^{-7}$	24	SPW	5	8.0
BODA-SPW-Zn5	$1.2{\cdot}10^{-4}$	$3.7{\cdot}10^{-6}$	58	SPW	2	8.0

no deviation from the reference isotherm. Based on the modelling indicated by the coloured solid lines in Fig. 1, Zn in sample IdP-Zn1 should be occupying essentially the so-called strong sites (high-affinity/low-capacity) whereas IdP-Zn2 sample should be an equal mix of Zn on the strong and weak sites (low affinity/high capacity). In the samples IdP-Zn3 and IdP-Zn4, Zn should be located mainly on the weak sites.

4.2. EXAFS results on illite

The $k^3\chi(k)$ EXAFS spectra obtained for intrinsic Zn in IdP (IdP-Zn_{incor}) and Zn adsorbed on the Idp-Zn1 (1w) and Idp-Zn1 (2y) samples are very similar (Fig. 2a). Especially the split beat pattern at 3.8 $Å^{-1}$, which is characteristic for Zn atoms located in octahedral layers of 2:1 phyllosilicates (Schlegel et al., 2001c; Dähn et al., 2011) is almost identical for IdP-$Zn_{incor,}$ Idp-Zn1 (1w) and Idp-Zn1 (2y). This indicates that the amount of 2.1 mmol/kg Zn taken up is sorbed to edge positions which have a very similar coordination environment as Zn atoms incorporated in the structure. With increasing Zn loading, the splitting of the oscillations at 3.8 $Å^{-1}$ is less pronounced (Fig. 2b). A similar behaviour has been observed in a P-EXAFS study by Dähn et al (2011) on the effect of surface loading by Zn on montmorillonite.

In the corresponding radial structure functions (RSFs) for the IdP-incorporated clay (IdP-Zn_{incor}) and the Zn treated IdP samples (Fig. 2c), there is a RSF peak (Zn—O contribution) at $R + \Delta R = 1.54$ Å. With increasing metal loading, the amplitude of this peak slightly decreases, while the peak position remains constant. Beyond the first shell, there are further RSF peaks in the $R + \Delta R$ range between 2 and 4 Å. Most of the variations observed in the $k^3\chi(k)$ spectra are transferred to the RSF in the range between 2 and 3.0 Å (Fig. 2c). The peaks at $R + \Delta R = 3$ and 3.8 Å are present in all samples, and their intensity decreases with increasing Zn loading. This indicates that with increasing loading the surface complexes at the IdP edge sites are becoming less ordered (Dähn et al., 2003; Dähn et al., 2011).

Data analysis showed that in the IdP-Zn_{incor} sample Zn is surrounded by one O shell at 2.07 Å, one Al Shell at 3.02 Å and one Si shell at 3.25 Å (Table 6, Fig. 2d). This local structure is characteristic of octahedral Zn in a 2:1 phyllosilicate environment (Schlegel et al., 2001c). The fact that only one Zn—Si backscattering pair is observed, is consistent with a C2/m-symmetry structure in trans-vacant clays (Tsipursky and Drits, 1984; Dähn et al., 2011). Montmorillonite with a cis-vacant structure (C2 symmetry) exhibit two Ni/Zn—Si backscattering pairs as observed by previous studies (Dähn et al., 2003; Dähn et al., 2011). Fur-

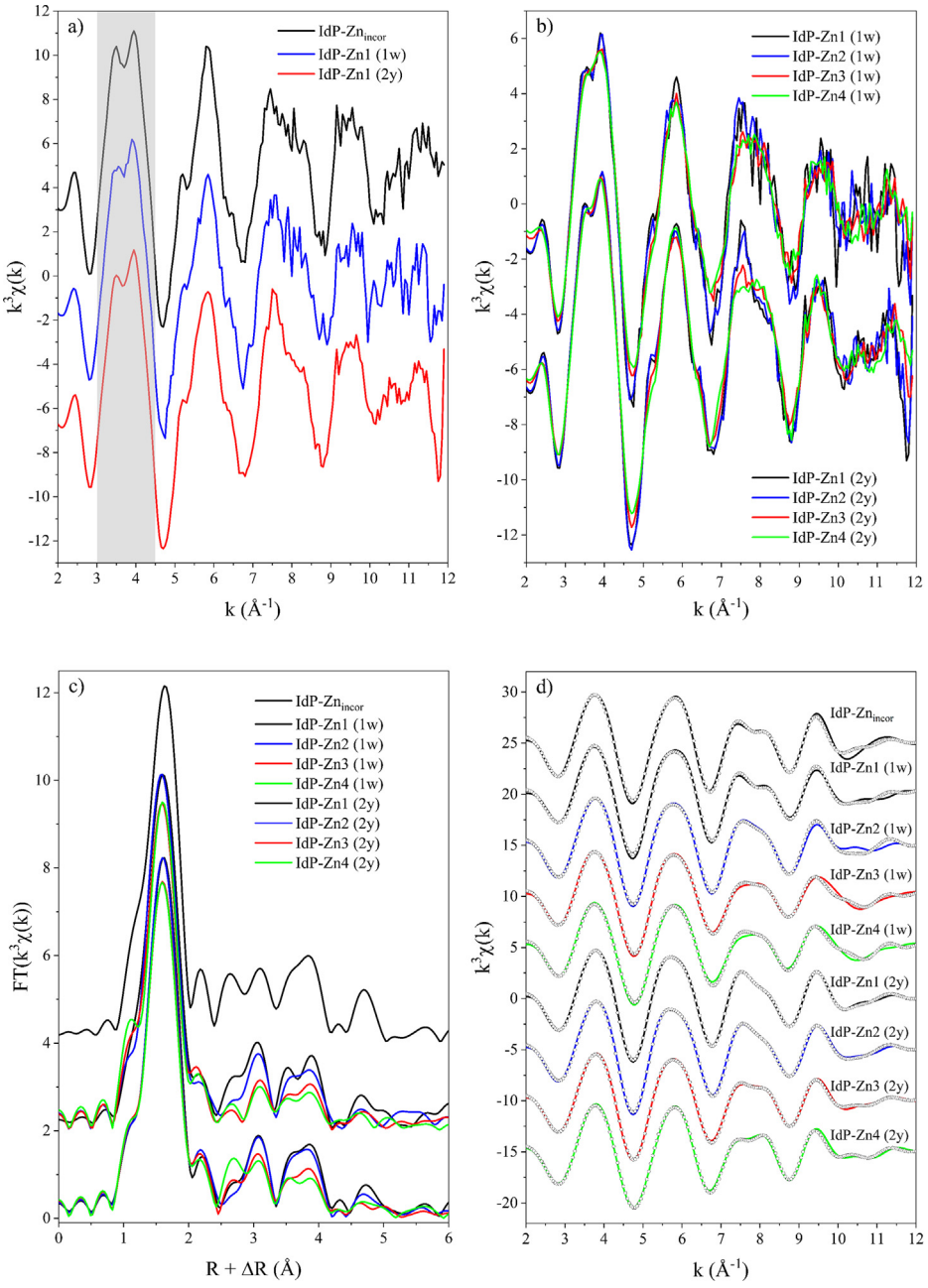

Fig. 2. (a) Comparison of k^3-weighted Zn K-edge EXAFS spectra of IdP-Zn$_{incor}$, Idp-Zn1 (1w) and Idp-Zn1 (2y), shaded area indicates the appearance of distinct features characteristic for Zn atoms located in octahedral layers of 2:1 phyllosilicates (Dähn et al., 2011), (b) k^3-weighted Zn K-edge EXAFS spectra of the Zn treated IdP samples, (c) the corresponding RSFs and (d) least-squares fit of FT^{-1} EXAFS data.

ther, the analysis showed that Zn is surrounded by 2.5(9) Al at 3.02(3) Å and 4.4(9) Si at 3.25(1) Å. In ideal dioctahedral smectites, $CN_{Zn-Al} = 3.0$ and $CN_{Zn-Si} = 4$ would be expected at distances between 3.0–3.1 Å and 3.2–3.3 Å, respectively (Güven, 1988). The fact that Zn appears to be surrounded by ~3 Al, and not 6, in the IdP-incorporated sample further indicates that Zn substitutes for Al and does not fill an empty site from the dioctahedral aluminium sheet. A similar observation was made by Manceau et al. (2005) and Vespa et al. (2010) for Red Hill montmorillonite, and for Zn in montmorillonite by Dähn et al. (2011). The additional peaks in the range $R + \Delta R = 3$–4 Å are caused by long Zn—O (at ~3.78 Å) and long Zn—Si-tetrahedral distances (at ~4.4 Å) (Manceau et al., 2000; Schlegel et al., 2001c; Schlegel and Manceau, 2006).

Data analysis for the Zn samples after 1 week reaction time indicates that CN_{Zn-Al}, R_{Zn-Al} and R_{Zn-Si} are within

Table 6
Results from the analysis of EXAFS data.

	Zn—O			Zn—Al			Zn—Zn			Zn—Si				Reduced χ^2	R-factor
	CN	*R* (Å)	σ^2 (Å^2)	*CN*	*R* (Å)	σ^2 (Å^2)	*CN*	*R* (Å)	σ^2 (Å^2)	*CN*	*R* (Å)	σ^2 (Å^2)	ΔE_0 (ev)		
Intrinsic Zn															
IdP-Zn$_{incor}$	6.4(5)	2.07(1)	0.009(2)	2.5(9)	3.02(3)	0.009(4)				4.4(9)	3.25(1)	0.009(4)[a]	3.1(9)	2309	0.02
OPA-Zn$_{incor}$	5.1(7)	2.06(1)	0.008(2)	3.0(1.2)	3.03(1)	0.008(3)				2.5(9)	3.29(2)	0.008(3)[a]	4.2(9)	1451	0.02
BODA-Zn$_{incor}$	6.0(8)	2.07(1)	0.008(2)	2.6(8)	3.04(2)	0.010(2)				1.9(9)	3.30(2)	0.010(2)[a]	4.0(9)	1837	0.02
Illite 1 week reaction															
IdP-Zn1 (1w)	6.2(4)	2.07(1)	0.009(2)	2.0(6)	3.02(3)	0.009(4)				4.0(7)	3.24(1)	0.009(4)[a]	3.4(6)	1092	0.02
IdP-Zn2 (1w)	6.2(4)	2.06(1)	0.009(2)[b]	2.0(6)	3.04(2)	0.009(4)[b]				3.4(7)	3.25(1)	0.009(4)[b]	3.4(6)[b]	1036	0.01
IdP-Zn3 (1w)	5.8(3)	2.06(1)	0.009(2)[b]	1.6(5)	3.06(3)	0.009(4)[b]				2.4(5)	3.26(2)	0.009(4)[b]	3.4(6)[b]	1986	0.01
IdP-Zn4 (1w)	5.7(3)	2.06(1)	0.009(2)[b]	1.5(5)	3.06(3)	0.009(4)[b]				2.3(5)	3.27(2)	0.009(4)[b]	3.4(6)[b]	2445	0.01
Illite 2 years reaction															
IdP-Zn1 (2y)	6.0(3)	2.06(1)	0.008(2)	2.1(5)	3.03(2)	0.008(4)				3.6(5)	3.24(1)	0.008(4)[a]	3.9(7)	1617	0.02
IdP-Zn2 (2y)	5.9(3)	2.06(1)	0.008(2)[b]	2.1(5)	3.04(2)	0.008(4)[b]				3.4(6)	3.24(2)	0.008(4)[b]	3.9(7)[b]	1690	0.02
IdP-Zn3 (2y)	5.6(3)	2.06(1)	0.008(2)[b]	2.0(5)	3.04(2)	0.008(4)[b]				3.1(5)	3.25(1)	0.008(4)[b]	3.9(7)[b]	3012	0.01
IdP-Zn4 (2y)	5.5(3)	2.06(1)	0.008(2)[b]	2.0(5)	3.03(1)	0.008(4)[b]				3.0(5)	3.27(1)	0.008(4)[b]	3.9(7)[b]	4934	0.01
OPA 1 week reaction															
OPA-NaCl-Zn1	5.7(9)	2.06(1)	0.008(2)	3.4(9)	3.03(1)	0.006(4)				1.4(9)	3.28(3)	0.006(4)[a]	2.6(9)	2675	0.02
OPA-NaCl-Zn2	5.9(9)	2.06(1)	0.008(2)[b]	3.2(6)	3.02(1)	0.006(4)[b]				1.0(6)	3.28(5)	0.006(4)[b]	2.6(9)[b]	3645	0.02
OPA-NaCl-Zn3	5.4(9)	2.06(1)	0.008(2)[b]	2.8(7)	3.01(2)	0.006(4)[b]				2.5(8)	3.30(4)	0.006(4)[b]	2.6(9)[b]	2963	0.02
OPA-NaCl-Zn3	5.6(9)	2.06(1)	0.008(2)[b]	2.8(9)	3.05(5)	0.006(4)[b]	1.4(9)	3.05(5)[a]	0.006(4)[a]	1.6(9)	3.33(9)	0.006(4)[b]	2.6(9)[b]	2089	0.02
OPA-NaCl-Zn4	5.5(9)	2.06(1)	0.008(2)[b]	2.5(7)	3.03(2)	0.006(4)[b]				3.5(8)	3.29(2)	0.006(4)[b]	2.6(9)[b]	3645	0.02
OPA-NaCl-Zn4	5.6(9)	2.06(1)	0.008(2)[b]	2.5(6)	3.05(2)	0.006(4)[b]	1.3(5)	3.05(2)[a]	0.006(4)[a]	3.0(9)	3.33(8)	0.006(4)[b]	2.6(9)[b]	3231	0.02
OPA-SPW-Zn1	5.5(8)	2.06(1)	0.008(2)	3.5(6)	3.03(1)	0.006(4)				1.7(6)	3.28(3)	0.006(4)[a]	3.0(9)	1465	0.02
OPA-SPW-Zn2	5.6(7)	2.06(1)	0.008(2)[b]	3.4(6)	3.02(1)	0.006(4)[b]				1.5(6)	3.27(3)	0.006(4)[b]	3.0(9)[b]	1626	0.02
OPA-SPW-Zn3	5.4(8)	2.06(1)	0.008(2)[b]	2.6(5)	3.02(2)	0.006(4)[b]				1.8(6)	3.29(2)	0.006(4)[b]	3.0(9)[b]	4885	0.02
OPA-SPW-Zn3	5.4(8)	2.05(1)	0.008(2)[b]	2.8(7)	3.05(2)	0.006(4)[b]	1.0(9)	3.05(2)[a]	0.006(4)[a]	1.4(9)	3.34(9)	0.006(4)[b]	3.0(9)[b]	4507	0.02
OPA-SPW-Zn4	5.5(9)	2.06(1)	0.008(2)[b]	2.6(7)	3.01(2)	0.006(4)[b]				2.6(7)	3.28(2)	0.006(4)[b]	3.0(9)[b]	5145	0.05
OPA-SPW-Zn4	5.5(9)	2.05(1)	0.008(2)[b]	2.7(9)	3.05(2)	0.006(4)[b]	1.4(9)	3.05(2)[a]	0.006(4)[a]	1.8(9)	3.34(9)	0.006(4)[b]	3.0(9)[b]	4283	0.05
BODA 1 week reaction															
BODA-NaCl-Zn1	5.8(7)	2.06(1)	0.009(2)	3.7(9)	3.05(1)	0.010(4)				3.3(9)	3.29(1)	0.010(4)[a]	2.1(9)	1668	0.01
BODA-NaCl-Zn2	5.6(6)	2.06(1)	0.009(2)[b]	3.4(7)	3.05(2)	0.010(4)[b]				2.6(8)	3.30(2)	0.010(4)[b]	2.1(9)[b]	1496	0.02
BODA-NaCl-Zn3	5.9(7)	2.06(1)	0.009(2)[b]	3.9(7)	3.03(2)	0.010(4)[b]				4.4(7)	3.28(1)	0.010(4)[b]	2.1(9)[b]	2129	0.01
BODA-NaCl-Zn3	5.9(9)	2.06(1)	0.009(2)[b]	3.9(9)	3.05(2)	0.010(4)[b]	1.0(9)	3.05(2)[a]	0.010(4)[a]	3.7(9)	3.30(4)	0.010(4)[b]	2.1(9)[b]	2511	0.01
BODA-NaCl-Zn4	6.0(9)	2.06(2)	0.009(2)[b]	3.9(9)	3.02(2)	0.010(4)[b]				5.7(9)	3.28(2)	0.010(4)[b]	2.1(9)[b]	7390	0.02
BODA-NaCl-Zn4	6.3(9)	2.06(2)	0.009(2)[b]	4.0(9)	3.05(2)	0.010(4)[b]	1.6(9)	3.05(2)[a]	0.010(4)[a]	4.6(9)	3.30(2)	0.010(4)[b]	2.1(9)[b]	7217	0.02
BODA-SPW-Zn1	5.3(7)	2.05(1)	0.009(2)	3.2(8)	3.05(2)	0.009(4)				2.7(9)	3.30(1)	0.009(4)[a]	2.7(9)	800	0.01
BODA-SPW-Zn2	5.6(7)	2.05(1)	0.009(2)[b]	3.0(7)	3.05(2)	0.009(4)[b]				2.5(8)	3.30(2)	0.009(4)[b]	2.7(9)[b]	1973	0.02
BODA-SPW-Zn3	5.6(8)	2.06(1)	0.009(2)[b]	3.6(8)	3.03(2)	0.009(4)[b]				3.9(9)	3.29(2)	0.009(4)[b]	2.7(9)[b]	2504	0.02
BODA-SPW-Zn4	6.0(9)	2.06(2)	0.009(2)[b]	4.1(9)	3.01(2)	0.009(4)[b]				6.0(9)	3.30(2)	0.009(4)[b]	2.7(9)[b]	7762	0.02
BODA-SPW-Zn4	6.0(9)	2.06(2)	0.009(2)[b]	4.2(9)	3.05(5)	0.009(4)[b]	1.6(9)	3.05(5)[a]	0.009(4)[a]	4.7(9)	3.32(7)	0.009(4)[b]	2.7(9)[b]	6267	0.02
BODA-SPW-Zn5	5.9(9)	2.06(2)	0.009(2)[b]	4.1(8)	3.01(2)	0.009(4)[b]				6.4(9)	3.30(2)	0.009(4)[b]	2.7(9)[b]	4973	0.02
BODA-SPW-Zn5	6.0(9)	2.05(2)	0.009(2)[b]	4.2(9)	3.05(5)	0.009(4)[b]	2.0(9)	3.05(5)[a]	0.009(4)[a]	5.4(9)	3.32(7)	0.009(4)[b]	2.7(9)[b]	4191	0.02

CN, *R*, σ^2, ΔE_0: coordination number, interatomic distance, Debye-Waller factor, shift of the threshold energy.
Precisions are shown in brackets (1 std). S_0^2 was fixed to 0.85.
All fits were performed in FT^{-1} between 1 and 3.4 Å. Reduced $\boldsymbol{\chi^2}$ and the R-factor are defined in IFEFFIT (Newville, 2001; Ravel and Newville, 2005)
[a] Correlated to the value of σ^2_{Zn-Al}(Zn1).
[b] Fixed to the value determined for the lowest Zn concentration.

the experimental error similar with increasing loading, only for the CN_{Zn-Si} a small decrease was observed (IdP-Zn1 (1w): $CN_{Zn-Al} = 2.0(6)$), $R_{Zn-Al} = 3.02(3)$ Å, $CN_{Zn-Si} = 4.0$ (7), $R_{Zn-Si} = 3.24(1)$ Å vs. IdP-Zn4 (1w): $CN_{Zn-Al} = 1.5$ (5), $R_{Zn-Al} = 3.06(3)$ Å, $CN_{Zn-Si} = 2.3(5)$, $R_{Zn-Si} = 3.27$ (2) Å; Table 6). The obtained structural parameters for the samples for a reaction time of two years are nearly independent of the loading (e.g. IdP-Zn1 (1y): $CN_{Zn-Al} = 2.1$ (5), $R_{Zn-Al} = 3.03(2)$ Å, $CN_{Zn-Si} = 3.6(5)$, $R_{Zn-Si} = 3.24$ (1) Å vs. IdP-Zn4 (1y): $CN_{Zn-Al} = 2.0(5)$, $R_{Zn-Al} = 3.03$ (1) Å, $CN_{Zn-Si} = 3.0(5)$, $R_{Zn-Si} = 3.27(1)$ Å) indicating that with extended reaction times the surface complexes tend to be more ordered (Dähn et al., 2003).

5. RESULTS: ZN – ARGILLACEOUS ROCKS

5.1. Sorption on Opalinus Clay and Boda Claystone

Sorption isotherms of Zn on OPA and BODA in their respective synthetic porewaters at pH ~ 8.0, (Table 5) were carried out over a $[Zn]_{eql}$ range from ~10^{-9} to 10^{-4} M (OPA) or ~10^{-9} to ~10^{-5} M (BODA) (Fig. 3). The 2SPNE SC/CE model for illite with the parameters given in Table 1 was used to blindly predict the sorption of Zn on the argillaceous rocks. The calculations considered the respective illite and illite/smectite mixed layer content (Table 2) and the porewater chemistry of OPA and BODA (Table 3).

5.2. EXAFS on Opalinus Clay and Boda Claystone

The $k^3\chi(k)$ EXAFS spectra of intrinsic Zn (Zn_{incor}) in IdP, OPA and BODA samples are very similar (Fig. 4a). The split in the oscillation at 3.8 $Å^{-1}$ is slightly stronger in the BODA sample compared to IdP and OPA. Since this split is absent in the FT^{-1} spectra of the IdP, OPA and BODA samples it indicates that this spectral feature is caused by the presence of higher atomic shells >4.0 Å. The spectra indicate that the Zn intrinsically present in the samples is located in the octahedral sheets of the clay platelets (Dähn et al., 2011). The spectra of the low loaded OPA and BODA samples show remarkable similarities, indicating that in both uptake systems the formation of similar inner-sphere complexes prevails (Fig. 4b). In addition, there is no difference at Zn loadings of 1.7–7.1 mmol/kg between OPA and BODA samples prepared in NaCl or in SPW (Fig. 4 c, f). With increasing Zn loading similar effects as in the case on Zn uptake by IdP are observed, e.g. the splitting of the oscillations at 3.8 $Å^{-1}$ is gradually attenuated (Fig. 4c, f).

For the samples with higher loadings (≥16 mmol/kg OPA; ≥24 mmol/kg BODA), the oscillation at ~8 $Å^{-1}$ shows a clear splitting, indicating the formation of Zn-precipitates (Schlegel et al., 2001a). In the BODA-SPW-Zn3 sample first indications of a splitting at ~8 $Å^{-1}$ are observed, suggesting that the fomation of Zn-precipitates in SPW can start already at Zn loadings of ~10 mmol/kg.

This feature is absent in the highest loaded Zn IdP samples (42 mmol/kg), even up to a reaction time of 2 years, which may indicate that the mineral composition of the argillaceous rocks plays an important role in the process of formation of secondary phases. Comparing the highest concentrated OPA and BODA samples seems to indicate that in this uptake system, the use of SPW favours the formation of precipitates compared to the use of NaCl (Fig. 4c, f).

The formation of Zn precipitates in the highest concentrated samples is further illustrated in the corresponding RSFs (Fig. 4d, g), were a strong RSF peak is observed at $R + \Delta R = 2.54$ Å. At low metal loadings further RSF peaks in the range $R + \Delta R$ between 2 and 4 Å are present.

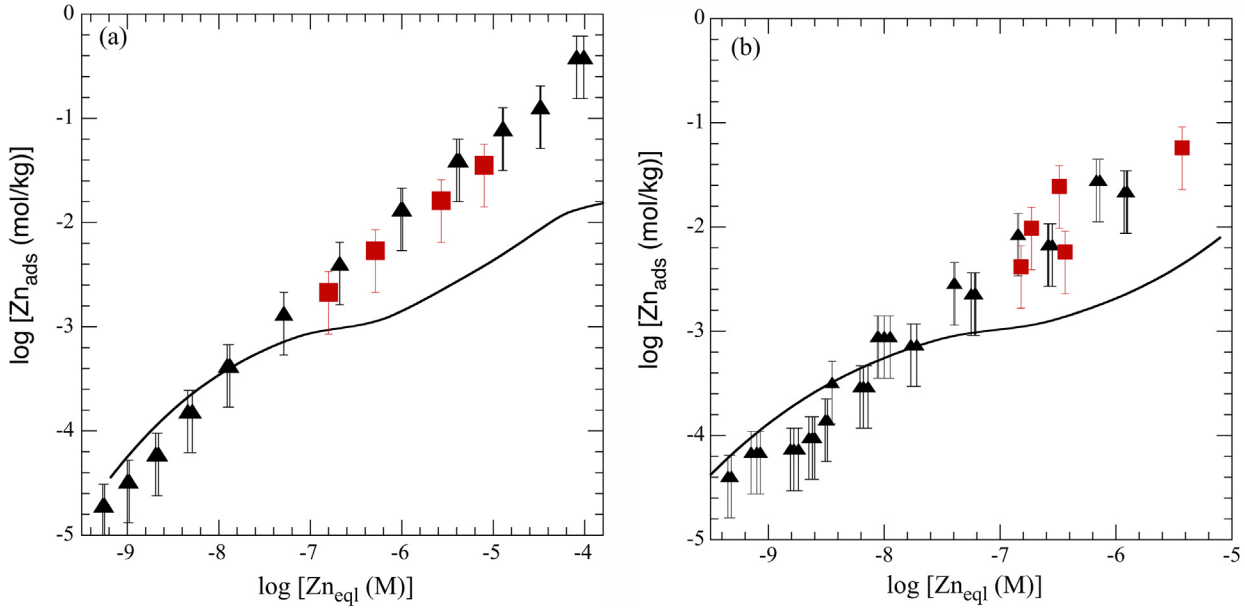

Fig. 3. Zn sorption isotherm in SPW on (a) OPA and (b) BODA; (▲) experimental results. Black continuous lines: blind prediction. (■) EXAFS samples.

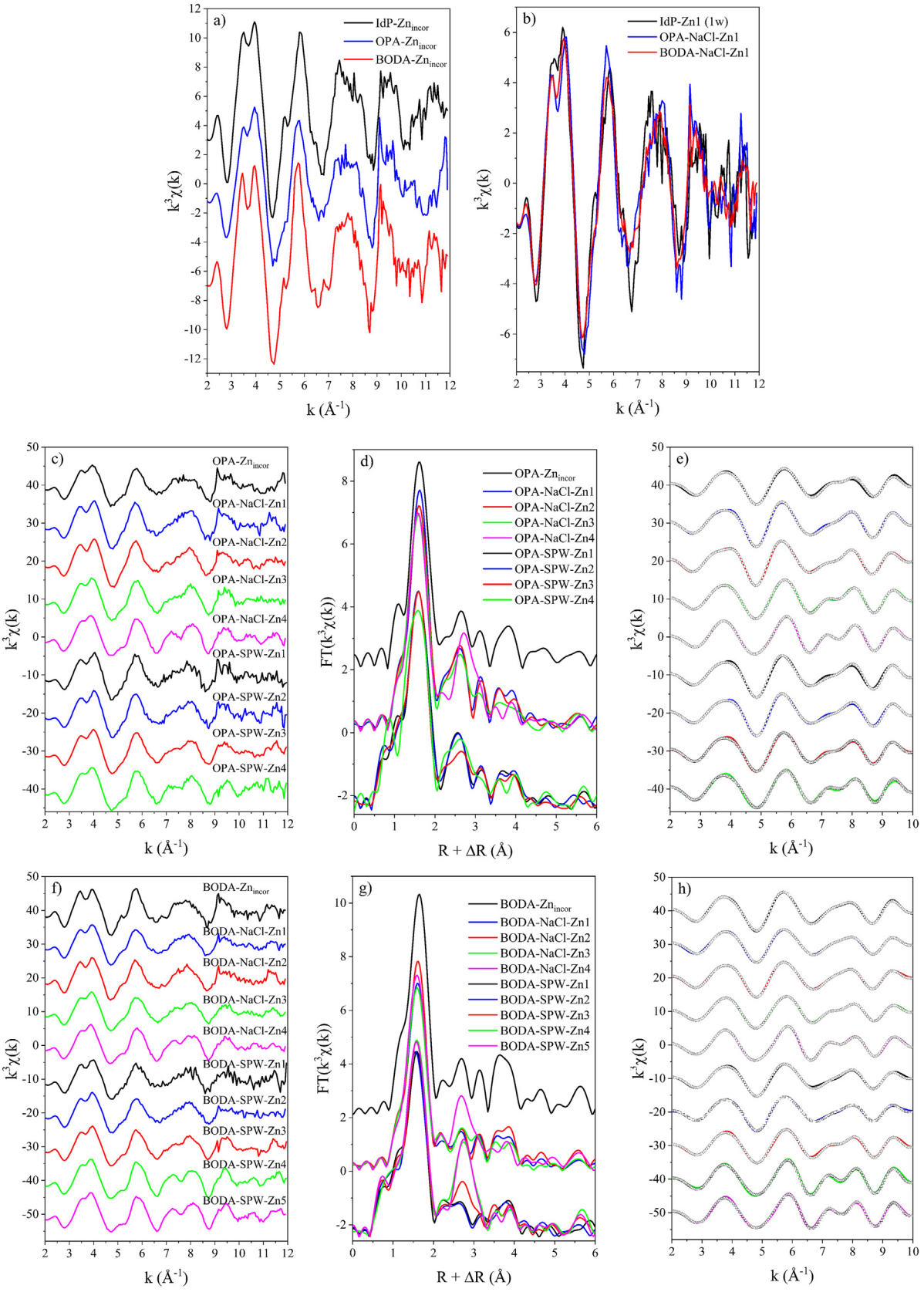

Fig. 4. (a) Comparison of k^3-weighted Zn K-edge EXAFS spectra of pure IdP, OPA and BODA in NaCl and SPW, (b) IdP-Zn1 (1w), OPA-NaCl-Zn1 and BODA-NaCl-Zn1, (c) k^3-weighted Zn K-edge EXAFS spectra of the Zn treated OPA samples, (d) the corresponding RSFs, (e) least-squares fit of FT^{-1} EXAFS data, (f) k^3-weighted Zn K-edge EXAFS spectra of the Zn-treated BODA samples, g) the corresponding RSFs, (h) least-squares fit of FT^{-1} EXAFS data.

Data analysis for the OPA and BODA samples with only intrinsic Zn indicate that ~3 Zn—Al backscattering pairs are present (Table 6). This indicates that Zn is located in the octahedral sheets of the dioctahedral clays and is not filling empty octahedral position (in this case 6 would be expected). The observed CN_{Zn-Si}(OPA) = 2.5(9) and CN_{Zn-Si}(BODA) = 1.9(9) are smaller compared to the value obtained for pure IdP (4.4(9)), and are also smaller than the theoretical expected 4 indicating a higher disorder compared to the IdP system.

The CN_{Zn-Al} and CN_{Zn-Si} of the OPA and BODA samples are within the eperimental error very similar and independent of the background (NaCl and SPW) solution (Table 6). The Zn—Al and Zn—Si bond distances agree well, within the uncertainties, with the values obtained for the pure systems. The R_{Zn-Al} all of the OPA and BODA samples are in the range between 3.01(2) Å and 3.05(2) Å. The R_{Zn-Si} all of the OPA and BODA samples are in the range between 3.27(3) Å and 3.34(9) Å. These distances are within uncertainties comparable to the ones obtained for the IdP system (Al: 3.02(3)–3.06(3), Si: 3.24(1)–3.27(2) Å). However, comparing the FT^{-1} spectra these differences in Zn—Si distances seems to be real, since the oscillation at ~8 $Å^{-1}$ shows an upward trend for OPA and BODA, whereas in the IdP system, except for the IdP-Zn4 (2y) sample, the right shoulder of the oscillation is lower than the left one (Fig. 2d, Fig. 4h, e).

The spectra of the samples in NaCl background electrolyte OPA-NaCl-Zn3, OPA-NaCl-Zn4, BODA-NaCl-Zn3 and BODA-NaCl-Zn4, and in SPW background electrolyte OPA-SPW-Zn3, OPA-SPW-Zn4, BODA-SPW-Zn4 and BODA-SPW-Zn5 were also fitted with a model considering Zn—Zn backscattering pairs as already indicated by the $k^3\chi(k)$ EXAFS spectra. The CN_{Zn-Zn} in all samples were in the range of 1.0(9) to 2.0(9). The R-factor indicating the goodness of the fit did not improve compared to fits without Zn—Zn backscattering pairs, indicating that Zn—Zn backscattering pairs are not significantly present in the samples.

6. DISCUSSION

In this study, the sorption of Zn on two argillaceous rocks, Opalinus Clay (OPA) and Boda Claystone (BODA), in 0.1 M NaCl and in their respective porewaters was investigated, by combining batch sorption experiments and sorption modelling. The sorption isotherms were blindly predicted with the 2SPNE SC/CE sorption model of Zn on Na-IdP by up-scaling to only the 2:1-clay mineral content and considering the aqueous speciation of Zn. The sorption of Zn on both rock samples exhibits a similar behaviour as Co and Ni on the same rock samples (Marques Fernandes et al., 2015). At $[Zn]_{eql} < \sim 10^{-7}$ M, the agreement between experimental data and the predictive modelling is within the experimental error bars of ±60%; whereas at $[Zn]_{eql} > \sim 10^{-7}$ M, the model calculations deviate increasingly from the experimental measurements (up to one order of magnitude at the highest $[Zn]_{eql}$). The Zn uptake in the region where it deviates from the model prediction is not due to aqueous solubility limits. In fact, the log R_d value in case of precipitation of a Zn solid phase such as Zn-hydroxides, -oxides or –carbonates from a supersaturated aqueous phase would sharply increase at a certain solubility limiting concentration and not gradually increase. Thermodynamic calculations and experimental verification confirm that even the highest Zn concentration is stable in the respective porewater. EXAFS data obtained for Ni on both argillaceous rocks in a previous study clearly evidenced that in the deviating region surface complexation is no longer the dominant retention mechanisms rather the formation of a new phase (Marques Fernandes et al., 2015). This process is likely to be the same which governs the uptake of Zn on OPA and BODA in the given concentration range. Remarkable is that such process would already begin at comparatively low metal concentrations (Dähn et al., 2001; Dähn et al., 2002a; Dähn et al., 2002b; Dähn et al., 2006; Schlegel and Manceau, 2006).

The 2SPNE SC/CE sorption model for illite with its non-adjustable parameters (site types and capacities, acid base and cation exchange reactions) can be regarded as very robust and is capable to quantitatively describe sorption of a whole suite of metals comprising Co, Ni, Zn, Eu, Am, Th and U. The simplified "bottom-up" approach predicted the uptake of Zn on the natural rocks with different mineralogy and porewater compositions at low concentrations ($[Zn]_{eql} < 10^{-7}$ M) well. However, at $[Zn]_{eql}$ above 10^{-7} M the calculations clearly underpredicted the sorption. In case of U, Th and Eu, this methodology has shown to be reliable over the whole measurable concentration range. For the divalent transition metal ions Zn, Co and Ni, surface complexation is apparently occurring only in a limited concentration range and consequently the applicability of this simplified approach, which presupposes surface complexation as the controlling uptake mechanism, has a limited validity.

In the application of the "bottom -up" approach in this study, only Zn adsorption on clay minerals is included since the thermodynamic model used can only describe adsorption processes. The "bottom-up" approach can be implemented by considering other relevant mechanisms contributing to the retention of (radio)contaminants. For instance, processes such as neo-formation, secondary phase formation or incorporation would improve the approach, however, these processes are yet not well understood and are not easy to model thermodynamically. Hence, there is still need for research in this field. Nevertheless, not considering additional uptake processes, is a conservative approach in the safety analysis.

The EXAFS results support findings based on wet chemistry calculations using the 2SPNE SC/CE model. Similar to a P-EXAFS study of Dähn et al. (2011) on the uptake of Zn by montmorillonite, the Zn illite system exhibit structural parameters consistent with the strong and weak site concept postulated in the 2SPNE SC/CE model. The nature of these strong an weak sites was elucidated by *ab initio* molecular dynamics simulations to investigate the structure and the stability of the edge surfaces of trans- and cis-vacant montmorillonites (Churakov and Dähn, 2012; Kéri et al., 2020). In the IdP system with prolonged reaction times of up to two years, no formation of Zn precipitates

were observed. This indicates that the Zn complexes are stable over a time period of two years, and dissolution and recrystallization processes might not play a significant role in the Zn-IdP uptake system. In contrary, in the OPA and BODA uptake system, precipitation processes could start to play a role at metal loadings higher than 16 mmol/kg (OPA) and 24 mmol/kg (BODA). However the observed structural parameters do not allow to unequivocally distinguish what kind of precipitate has formed. Possible candidates include Zn-phyllosilicates (Dähn et al., 2001, 2002b; Jacquat et al., 2008; Schlegel et al., 2001b, 2001c), Zn-LDH (Scheidegger et al., 1998; Scheinost et al., 1999), hydrozincite (Zachara et al., 1989; Lee et al., 2005) and zinc carbonate (Zachara et al., 1989; Elzinga and Reeder, 2002; Lee et al., 2005). The observed Si concentrations in solution in all uptake systems of this study were in the range between $8.3{\cdot}10^{-5}$ M and $2.25{\cdot}10^{-4}$ M (see Table SI-2). In studies where the neoformation of Zn phyllosilicates were observed the Si concentrations exceeded $5.0{\cdot}10^{-4}$ M (Schlegel et al., 2001b; Dähn et al., 2002b). This indicates that the Si concentrations cannot play a significant role in the OPA and BODA uptake system and do not favour the neoformation of phyllosilicates. This is further supported by the fact that in the Zn-IdP uptake system with Si concentrations of ~$1.0{\cdot}10^{-4}$ M no indications for Zn—Zn backscattering pairs were observed. The presence of significant amounts of Zn-LDH phases can be ruled out based on the fact that a distinct feature, e.g. a split of the oscillation at ~8.0 $Å^{-1}$ in the k^3-weighted Zn K-edge EXAFS spectra is missing (Scheinost and Sparks, 2000; Dähn et al., 2002b). Furthermore, the predominant formation of a kerolite phase is not occuring, because k^3-weighted Zn K-edge EXAFS spectra of Zn-kerolite show a well separated oscillation at ~5.0 $Å^{-1}$ (Schlegel et al., 2001b; Schlegel et al., 2001c; Jacquat et al., 2008), which is missing in the spectra of the OPA and BODA samples. The formation of zinc carbonate ($ZnCO_3$) can be excluded because the EXAFS spectra are significantly different from the ones in this study (Elzinga and Reeder, 2002; Lee et al., 2005). In addition the solubility of hydrozincite ($Zn_5(OH)_6(CO_3)_2$) is lower than that of $ZnCO_3$ (Zachara et al., 1989), and thus a precipitation of hydrozincite would be favoured. Ghose (1964) determined with XRD for hydrozincite two Zn—Zn backscattering pairs of CN_{Zn-Zn} 2.3 and 5.2, at distances of 3.172 Å and 3.576 Å, respectively. Similar, Lee and Elzinga (2005) observed in an EXAFS study CN_{Zn-Zn} of 2.1 and 3.4, at distances of 3.15 Å and 3.54 Å, respectively. In this study only one Zn—Zn backscattering pair with CN_{Zn-Zn} between 1.0(9) and 2.0(9) at a distance of 3.05 (5) Å was observed. Therefore, based on different structural parameters as observed in this study, the predominant formation of hydrozincite in the OPA and BODA uptake systems can be ruled out. It therefore appears likely that not a single process is responsible for the beginning of precipitation processes in argillaceous rocks, and that rather a mixture of different newly formed phases can explain the experimental data.

The differences between argillaceous rock samples prepared in NaCl and SPW are modest under the employed reaction conditions indicating that in the case of Zn, the solid phase plays a predominant role in the uptake process, and that affects originating from the porewater are minor. The study demonstrated how results of "pure" systems such as IdP can be transferred to predict the uptake by argillaceous rocks at low sorbate concentrations. At elevated metal concentrations, the formation of secondary phases is favoured, which can significantly retard the migration in the geosphere.

Declaration of Competing Interest

The authors declare that they have no known competing financial interests or personal relationships that could have appeared to influence the work reported in this paper.

ACKNOWLEDGEMENT

The project received funding from the Swiss-Hungarian Cooperation Program through Project SH/7/2/11 and from the National Cooperative for the Disposal of Radioactive Waste (Nagra). The Public Limited Company for Radioactive Waste management (PURAM, Hungary) is acknowledged for providing the Boda Claystone sample. Experimental assistance by A. Schaible and E. Eltayeb are gratefully acknowledged. The help of the staff of the beamline 11-2 at the SSRL is gratefully acknowledged. Use of the Stanford Synchrotron Radiation Lightsource, SLAC National Accelerator Laboratory, is supported by the U.S. Department of Energy, Office of Science, Office of Basic Energy Sciences under Contract No. DE-AC02-76SF00515. The SSRL Structural Molecular Biology Program is supported by the DOE Office of Biological and Environmental Research, and by the National Institutes of Health, National Institute of General Medical Sciences (including P41GM103393). The contents of this publication are solely the responsibility of the authors and do not necessarily represent the official views of NIGMS or NIH.

APPENDIX A. SUPPLEMENTARY MATERIAL

Supplementary data to this article can be found online at https://doi.org/10.1016/j.gca.2021.07.001.

REFERENCES

Andra, 2001. Référentiel géologique du site de Meuse/Haute Marne, Châtenay-Malabry, France.

Ankudinov A. L., Ravel B., Rehr J. J. and Conradson S. D. (1998) Real-space multiple-scattering calculation and interpretation of x-ray-absorption near-edge structure. *Phys. Rev. B* **58**, 7565–7576.

Baes C. F. and Mesmer R. E. (1976) Hydrolysis of Cations. Wiley.

Baeyens B. and Bradbury M. H. (2004) Cation exchange capacity measurements on illite using the sodium and cesium isotope dilution technique: effects of the index cation, electrolyte concentration and competition: modeling. *Clays Clay Miner.* **52**, 421–431.

Bonin B. (1998) Deep geological disposal in argillaceous formations: studies at the Tournemire test site. *J. Contam. Hydrol.* **35**, 315–330.

Bradbury M. H. and Baeyens B. (2009a) Sorption modelling on illite Part I: Titration measurements and the sorption of Ni Co, Eu and Sn. *Geochim. Cosmochim. Acta* **73**, 990–1003.

Bradbury M. H. and Baeyens B. (2009b) Sorption modelling on illite. Part II: Actinide sorption and linear free energy relationships. *Geochim. Cosmochim. Acta* **73**, 1004–1013.

Bradbury M. H. and Baeyens B. (2011) Predictive sorption modelling of Ni(II), Co(II), Eu(IIII), Th(IV) and U(VI) on MX-80 bentonite and Opalinus Clay: A "bottom-up" approach. *Appl. Clay Sci.* **52**, 27–33.

Breitner D., Osán J., Fábián M., Zagyvai P., Szabó C., Dähn R., Fernandes M. M., Sajó I. E., Máthé Z. and Török S. (2015) Characteristics of uranium uptake of Boda Claystone Formation as the candidate host rock of high level radioactive waste repository in Hungary. *Environ. Earth Sci.* **73**, 209–219.

Chaney R. L. (1973) Crop and food chain effects of toxic elements in sludges and effluents. In *Recycling Municipal Sludges and Effluents on Land*, pp. 129–141.

Chen Z., Montavon G., Guo Z., Wang X., Razafindratsima S., Robinet J. C. and Landesman C. (2014) Approaches to surface complexation modeling of Ni(II) on Callovo-Oxfordian claystone. *Appl. Clay Sci.* **101**, 369–380.

Chumbley C. (1971) Permissible Levels of Toxic Metals in Sewage Used on Agricultural Land. Ministry of Agriculture, Fisheries and Food.

Churakov S. V. and Dähn R. (2012) Zinc adsorption on clays inferred from atomistic simulations and EXAFS spectroscopy. *Environ. Sci. Technol.* **46**, 5713–5719.

Dähn R., Baeyens B. and Bradbury M. H. (2011) Investigation of the different binding edge sites for Zn on montmorillonite using P-EXAFS – the strong/weak site concept in the 2SPNE SC/CE sorption model. *Geochim. Cosmochim. Acta* **75**, 5154–5168.

Dähn R., Jullien M., Scheidegger A. M., Poinssot C., Baeyens B. and Bradbury M. H. (2006) Identification of neoformed Ni-phyllosilicates upon Ni uptake in montmorillonite. A transmission electron microscopy and X-ray absorption fine structure study. *Clays Clay Miner.* **54**, 209–219.

Dähn R., Scheidegger A. M., Manceau A., Curti E., Baeyens B., Bradbury M. H. and Chateigner D. (2002a) Th uptake on montmorillonite: A powder and polarized extended x-ray absorption fine structure (EXAFS) study. *J. Colloid Interface Sci.* **249**, 8–21.

Dähn R., Scheidegger A. M., Manceau A., Schlegel M. L., Baeyens B. and Bradbury M. H. (2001) Ni clay neoformation on montmorillonite surface. *J. Synchrotron Radiat.* **8**, 533–535.

Dähn R., Scheidegger A. M., Manceau A., Schlegel M. L., Baeyens B., Bradbury M. H. and Chateigner D. (2003) Structural evidence for the sorption of Ni(II) atoms on the edges of montmorillonite clay minerals: a polarized X-ray absorption fine structure study. *Geochim. Cosmochim. Acta* **67**, 1–15.

Dähn R., Scheidegger A. M., Manceau A., Schlegel M. L., Baeyens B., Bradbury M. H. and Morales M. (2002b) Neoformation of Ni phyllosilicate upon Ni uptake on montmorillonite: A kinetics study by powder and polarized extended X-ray absorption fine structure spectroscopy. *Geochim. Cosmochim. Acta* **66**, 2335–2347.

Davis J. A., Coston J. A., Kent D. B. and Fuller C. C. (1998) Application of the surface complexation concept to complex mineral assemblages. *Environ. Sci. Technol.* **32**, 2820–2828.

De Haan F. and Zwerman P. (1976) Pollution of soil. *Dev. Soil Sci.* **5**, 192–271.

Elzinga E. J. and Reeder R. J. (2002) X-ray absorption spectroscopy study of Cu^{2+} and Zn^{2+} adsorption complexes at the calcite surface: Implications for site-specific metal incorporation preferences during calcite crystal growth. *Geochim. Cosmochim. Acta* **66**, 3943–3954.

Gabis V. (1958) Etude préliminaire des argiles oligocènes du Puy-en-Velay (Haute-Loire). *Bull. Soc. Franç. Minéral. Cristallog* **81**, 183–185.

Ghose S. (1964) The crystal structure of hydrozincite, $Zn_5(OH)_6(CO_3)_2$. *Acta Crystallogr. A* **17**, 1051–1057.

Güven N. (1988) Smectites. In *Hydrous Phyllosilicates (Exclusive Micas)* (ed. S. W. Bailey). Mineralogical Society of America, pp. 497–559.

Jacquat O., Voegelin A., Villard A., Marcus M. A. and Kretzschmar R. (2008) Formation of Zn-rich phyllosilicate, Zn-layered double hydroxide and hydrozincite in contaminated calcareous soils. *Geochim. Cosmochim. Acta* **72**, 5037–5054.

Kéri A., Dähn R., Marques Fernandes M., Scheinost A. C., Krack M. and Churakov S. (2020) Iron adsorption on clays inferred from atomistic simulations and XAS studies. *Environ. Sci. Technol.* **54**, 11886–11893.

Lázár K. and Máthé Z. (2012) Claystone as a potential host rock for nuclear waste storage. In *Clay Minerals in Nature – Their Characterization, Modification and Application* (eds. M. Valaškova and G. S. Martynkova). INTECH Open Access Publisher, Rijeka, Croatia.

Lee Y. J., Elzinga E. J. and Reeder R. J. (2005) Sorption mechanisms of zinc on hydroxyapatite: Systematic uptake studies and EXAFS spectroscopy analysis. *Environ. Sci. Technol.* **39**, 4042–4048.

Leeper G. W. (1972) Reactions of Heavy Metals with Soils with Special Regard to their Application in Sewage Wastes. DTIC Document.

Manceau A., Chateigner D. and Gates W. P. (1998) Polarized EXAFS, distance-valence least-squares modeling (DVLS) and quantitive texture analysis approaches to the structural refinement of Garfield nontronite. *Phys. Chem. Miner.* **25**, 347–365.

Manceau A., Lanson B., Schlegel M. L., Hargé J. C., Musso M., Eybert-Bérard L., Hazemann J. L., Chateigner D. and Lamble G. M. (2000) Quantitative Zn speciation in smelter-contaminated soils by EXAFS spectroscopy. *Am. J. Sci.* **300**, 289–343.

Manceau A., Marcus M. A. and Tamura N. (2002) Quantitative speciation of heavy metals in soils and sediments by synchrotron X-ray techniques. *Rev. Mineral. Geochem.* **49**, 341–428.

Manceau A., Tommaseo C., Rihs S., Geoffroy N., Chateigner D., Schlegel M., Tisserand D., Marcus M. A., Tamura N. and Chen Z.-S. (2005) Natural speciation of Mn, Ni, and Zn at the micrometer scale in a clayey paddy soil using X-ray fluorescence, absorption, and diffraction. *Geochim. Cosmochim. Acta* **69**, 4007–4034.

Marques Fernandes M. and Baeyens B. (2019) Cation exchange and surface complexation of lead on montmorillonite and illite including competitive adsorption effects. *Appl. Geochem.* **100**, 190–202.

Marques Fernandes M., Vér N. and Baeyens B. (2015) Predicting the uptake of Cs Co, Ni, Eu, Th and U on argillaceous rocks using sorption models for illite. *Appl. Geochem.* **59**, 189–199.

Mengel K. and Kirkby E. A. (1978) Principles of plant nutrition. *Principles of Plant Nutrition*.

Montoya V., Baeyens B., Glaus M. A., Kupcik T., Marques Fernandes M., Van Laer L., Bruggeman C., Maes N. and Schäfer T. (2018) Sorption of Sr, Co and Zn on illite: Batch experiments and modelling including Co in-diffusion measurements on compacted samples. *Geochim. Cosmochim. Acta* **223**, 1–20.

Nagra (2002) *Project Opalinus Clay: Safety Report. Demonstration of Disposal Feasibility (Entsorgungsnachweis) for Spent Fuel, Vitrified High-level Waste and Long-lived Intermediate-level Waste*. Nagra, Wettingen, Switzerland.

Newville M. (2001) IFFEFFIT: interactive XAFS analysis and FEFF fitting. *J. Synchrotron Radiat.* **8**, 322–324.

O'Day P. A., Brown, Jr., G. E. and Parks G. A. (1994) X-ray absorption spectroscopy of cobalt (II) multinuclear surface complexes and surface precipitates on kaolinite. *J. Colloid Interface Sci.* **165**, 269–289.

Ondraf/Niras, 2001. SAFIR 2: Safety Assessment and Feasibility Interim Report 2. Repord NIROND 2001-05E.

Pais I. and Jones, Jr, J. B. (1997) *The Handbook of Trace Elements*. CRC Press.

Payne T. E., Brendler V., Ochs M., Baeyens B., Brown P. L., Davis J. A., Ekberg C., Kulik D. A., Missana T., Tachi Y., Van Loon L. R. and Altmann S. (2013) Guidelines for thermodynamic sorption modelling in the context of radioactive waste disposal. *Environ. Model. Softw.* **42**, 143–156.

Poinssot C., Baeyens B. and Bradbury M. H. (1999) Experimental and modelling studies of caesium sorption on illite. *Geochim. Cosmochim. Acta* **63**, 3217–3227.

Ravel B. and Newville M. (2005) ATHENA, ARTEMIS, HEPHAESTUS: Data analysis for X-ray absorption spectroscopy using IFEFFIT. *J. Synchrotron Radiat.* **12**, 537–541.

Rehr J. J., Mustre de Leon J., Zabinsky S. and Albers R. C. (1991) Theoretical x-ray absorption fine structure standards. *J. Am. Chem. Soc.* **113**, 5135–5140.

Scheidegger A. M., Strawn D. G., Lamble G. M. and Sparks D. L. (1998) The kinetics of mixed Ni-Al hydroxide formation on clay and aluminum oxide minerals: A time-resolved XAFS study. *Geochim. Cosmochim. Acta* **62**, 2233–2245.

Scheinost A. C., Ford R. G. and Sparks D. L. (1999) The role of Al in the formation of secondary Ni precipitates on pyrophyllite, gibbsite, talc, and amorphous silica: A DRS study. *Geochim. Cosmochim. Acta* **63**, 3193–3203.

Scheinost A. C. and Sparks D. L. (2000) Formation of layered single- and double-metal hydroxide precipitates at the mineral/water interface: A multiple-scattering XAFS analysis. *J. Colloid Interface Sci.* **223**, 1–12.

Schlegel M. L. and Manceau A. (2006) Evidence for the nucleation and epitaxial growth of Zn phyllosilicate on montmorillonite. *Geochim. Cosmochim. Acta* **70**, 901–917.

Schlegel M. L., Manceau A. and Charlet L. (1999) Sorption of metal ions on clay minerals: 2. Mechanism of Co sorption on hectorite at high and low ionic strength and impact on the sorbent stability. *J. Colloid Interface Sci.* **220**, 392–405.

Schlegel M. L., Manceau A., Charlet L., Chateigner D. and Hazemann J. L. (2001a) Sorption of metal ions an clay minerals. 3. Nucleation and epitaxial growth of Zn phyllosilicate on the edges of hectorite. *Geochim. Cosmochim. Acta* **65**, 4155–4170.

Schlegel M. L., Manceau A., Charlet L., Chateigner D. and Hazemann J. L. (2001b) Sorption of metal ions on clay minerals. 3. Nucleation and epitaxial growth of Zn phyllosilicate on the edges of hectorite. *Geochim. Cosmochim. Acta* **65**, 4155–4170.

Schlegel M. L., Manceau A., Charlet L. and Hazemann J. L. (2001c) Adsorption mechanisms of Zn on hectorite as a function of time, pH, and ionic strength. *Am. J. Sci.* **301**, 798–830.

Sposito G. (2008) *The Chemistry of Soils*. Oxford University Press.

Tsipursky S. I. and Drits V. A. (1984) The distribution of octahedral cations in the 2:1 layers of dioctahedral smectites studied by oblique-texture electron diffraction. *Clay Miner.* **19**, 177–193.

Vespa M., Manceau A. and Lanson M. (2010) Natural attenuation of zinc pollution in smelter-affected soil. *Environ. Sci. Technol.* **44**, 7814–7820.

Zachara J. M., Kittrick J. A., Dake L. S. and Harsh J. B. (1989) Solubility and surface spectroscopy of zinc precipitates on calcite. *Geochim. Cosmochim. Acta* **53**, 9–19.

Associate editor: Annie B. Kersting